Fatigue Test of the Inconel Alloy 718 Under Three Point Bending Load at Low Frequency

J. Belan, L. Hurtalová, A. Vaško, E. Tillová and M. Chalupová

Abstract Inconel alloy 718 is a high-strength, corrosion-resistant, and hardenable Ni–Cr alloy with good tensile, fatigue, creep, and rupture strength which has resulted in its usage in a wide range of applications. It is used at temperatures ranging from −250 up to 705 °C. The main areas of application are the aircraft industry, as well as the space industry. Turbine-engine components experience significant fluctuations in stress and temperature during their repeated takeoff-cruise-landing cycles. These cycles can result in localized, small, plastic strains. Thus low-cycle, low-frequency fatigue is of interest to engine design. Engine vibrations and airflow between the stages of the turbine can also result in high-cycle fatigue with rapid cycle accumulation in airfoils at much higher frequencies, in the kHz range. This article deals with fatigue test of the IN 718 alloy under three point bending load at low frequency. Most of the fatigue tests for this alloy have been previously done under rotation bending loading, with the aim of comparing the results achieved in fatigue crack initiation and crack propagation. SEM microstructure and fractography analyses have also been carried out in this regard.

Keywords Inconel alloy 718 · Fatigue test · Three point bending · S-N curve · SEM fractography

J. Belan (✉) · L. Hurtalová · A. Vaško · E. Tillová · M. Chalupová
Faculty of Mechanical Engineering, Department of Materials Engineering,
University of Žilina, Univerzitná 8215/1, 01026 Žilina, Slovakia
e-mail: juraj.belan@fstroj.uniza.sk

L. Hurtalová
e-mail: lenka.hurtalova@fstroj.uniza.sk

A. Vaško
e-mail: alan.vasko@fstroj.uniza.sk

E. Tillová
e-mail: eva.tillova@fstroj.uniza.sk

M. Chalupová
e-mail: maria.chalupova@fstroj.uniza.sk

A. Öchsner and H. Altenbach (eds.), *Properties and Characterization of Modern Materials*, Advanced Structured Materials 33,
DOI 10.1007/978-981-10-1602-8_7

1 Introduction

This alloy was developed in the 1960s when the former Fe-based superalloys evolved towards Ni-based superalloys. Alloy 718 contains both Fe and Ni alloyed with some Al and Ti, though the most important addition is the refractory element Nb. The strength of the alloy 718 comes from coherent solid-state precipitates, which are for a small part γ'-Ni_3Al but mostly γ''-Ni_3Nb precipitates [1–6]. The major strengthening phases in the alloy 718 are the γ'' and γ' phases which produce coherency strains in the γ matrix. The γ'' phase is considered to be the main strengthening phase and has a DO_{22} BCT crystal structure, while the γ' phase is a FCC ordered phase with a Ll_2 crystal structure. The strengthening phases γ'' and γ' contain 3 atoms of Ni, while the γ'' phase is richer in Nb, while the γ' phase is richer in Al.

The γ'' and γ' phases have unique morphologies. The γ' phase precipitates as round particles with size less than 200 Å, and continues to be round in shape when it coalesces at higher temperatures. The γ'' phase rather takes the shape of a disk with a length of 5–6 times its thickness; however, when the γ'' phase precipitates at very low temperatures, a TEM is necessary to resolve its shape. The γ'' phase continues to grow in the disk shape at higher heat treatment temperatures or exposures. Some studies [7] have indicated that the γ'' and γ' phases grow in a sandwich-like morphology indicating a co-precipitation of the phases.

Because the γ''/γ' phases grow with higher temperatures and long time exposures at low temperatures, a transition of γ' to γ'' to delta phase occurs slowly at lower temperatures, but the reaction occurs faster or sooner at higher temperatures. Recent data [7] has indicated that the γ'' phase is the least stable phase and the transition goes through γ'' phase to delta phase and finally γ' phase.

The delta phase found in alloy 718 is incoherent with the γ and has an orthorhombic crystal structure. The delta phase is found mostly as plates growing on the (111) planes or nucleating on the grain boundaries, and is associated with loss of strength as well as loss of fatigue lifetime in this alloy. The delta phase in the grain boundaries is used to control the grain size in wrought materials and seems to also be important for notch ductility [7]. Figure 1 shows a typical microstructure of the wrought alloy 718. The microstructure consists of light grey blocks of carbides and fine lenticular and lamellar particles of delta phase (Ni_3Nb) distributed in the FCC matrix, with grain size approximately 10 μm and a few deformation twins.

During the past few decades, extensive investigations have been made on the low-cycle fatigue (LCF) and high-cycle fatigue (HCF) properties of IN718, such as the effect of temperature on the cyclic stress-strain response and LCF life associated with the deformation of microstructures [8–10], the factors (temperature, environment, and loading parameters, etc.) influencing fatigue crack growth [11–13], the creep-fatigue oxidation interactions [13, 14], the mechanism-based modelling of fatigue life prediction [15], etc. Nowadays, the very high-cycle fatigue (VHCF) properties of high-strength metals have become more and more significant, ever since the finding of fatigue failure beyond 10^7 cycles in high-strength steels [16]. The subsequent studies on many ferroalloys [17, 18] prove that the conventional

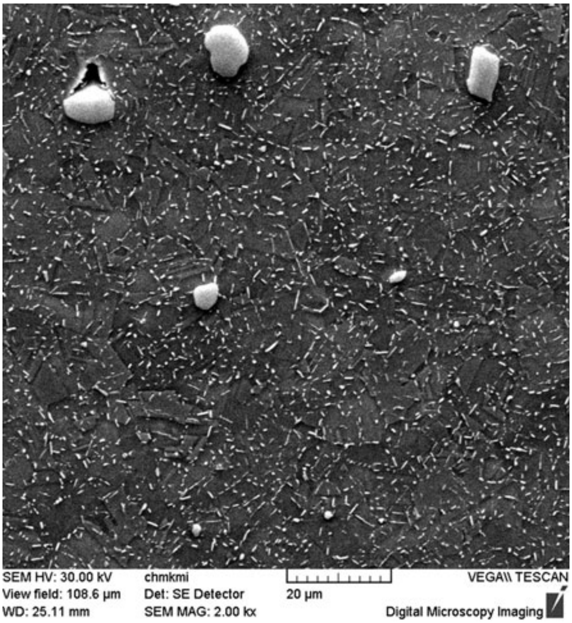

Fig. 1 The typical wrought INCONEL alloy 718 microstructure, SEM, etch. Kallings

fatigue limit in HCF disappears in the VHCF regime and there is a transition of fatigue crack initiation from the surface to the internal defects at around 10^6–10^7 cycles [19]. Furthermore, it is recognized that the gigacycle fatigue failure of high strength steels is preferentially initiated from interior inclusions, giving the appearance of a fish-eye [17, 18].

Compared to the comprehensive investigation and understanding of the VHCF properties of steels [19, 20] and Al-alloys [21], few studies exist on nickel-based superalloys, e.g. IN718 superalloy [22].

Yan et al. [22] performed a rotary bending fatigue test on IN718 and found that it did not show gigacycle fatigue failure at room temperature, but did at 500 °C. However, another study [23], under ultrasonic frequency, revealed that fatigue fracture of IN718 occurred between 10^7 and 10^8 cycles. As the experimental work suggests, it is still disputable whether this superalloy under practical loading would show VHCF or not. Furthermore, it is known that the fatigue crack initiation process becomes increasingly important with the extension of fatigue life.

In this study, the HCF properties of the IN718 superalloy were investigated under a three point flexure fatigue test at the average frequency f = 143–151 Hz and at room temperature. With the help of a scanning electron microscope (SEM), fractography analyses were performed to disclose the fracture features of samples in different life ranges. And finally the comparisons of ultrasonic push-pull fatigue test results to the three point flexure fatigue test results are given. Also the initiation and propagation of fatigue crack at various conditions of loading is discussed.

2 Experimental Materials and Methods

The material used in this study is a Ni-based superalloy INCONEL 718 with a chemical composition (in wt%) shown in Table 1.

The material was heat treated, according to the supplier's BIBUS Ltd. (CZ) material sheet, at 980 °C/1 h AC (air cooled) and heating at 720 °C/8 h followed FC (furnace cooled) (50 °C per hour) to temperature 620 °C holding time 8 h and air cooled. The achieved mechanical properties of the material with grain size ASTM 12 are in Table 2.

The experimental material for the three point flexure fatigue test was machined down into a simple blocky shape as reported in the schematic drawing (see Fig. 2). Also, for the calculation of the maximum bending stress, we used the formula (1):

$$\sigma_{omax} = \frac{3 \times F \times L}{2 \times b \times h^2} \quad \text{MPa} \tag{1}$$

where σ_{omax} is the maximum bending stress (MPa), F is the dynamic load (N), L is the distance of supports (mm), b is the specimens width (mm), and h is the sample height (mm).

The three point flexure fatigue test was carried out on testing machine ZWICK/ROELL Amsler 150 HFP 5100 at room temperature with a static pre-load $F_{static} = -15$ kN (this value may be considered as F_{medium} when dynamic load changes from maximum to minimum around this F_{medium}) and dynamic force $F_{dynamic}$ varies from 6.31 up to 12.8 kN. The value of 2×10^7 cycles was set as a reference and when the sample had reached this value without breaking, the so-called run-out, that bending stress was considered as the fatigue lifetime limit. The frequency of fatigue tests was approximately $f = 150$ Hz. The S-N curve was

Table 1 Chemical composition (in wt%) of INCONEL alloy 718

	C	Si	Mn	Al	Co	Cr	Mo	Nb	Ni	Ta	Ti
Btm	0.026	0.08	0.07	0.56	0.14	19.30	2.98	5.27	53.29	<0.01	0.95
Top	0.026	0.09	0.07	0.57	0.14	19.31	2.99	5.30	53.32	<0.01	0.96
Max	0.08	0.35	0.35	0.8	1.00	21.00	3.30	5.50	55.0	0.05	1.15

Fe content is the remainder

Table 2 Mechanical properties of INCONEL alloy 718 as received, according to BIBUS Ltd. material sheet

Temp. (°C)	Rp 0.2 (MPa)	Rm (MPa)	Elongation A (%)	Reduced area Z (%)	HBW 10/3000	$\sigma_{T/649}$ (MPa)	Rupture life (h)	A (%) creep
20	1213	1549	21.3	33.3	429	–	–	–
649	986	1123	22.6	68.0	–	689	26.8	45.7

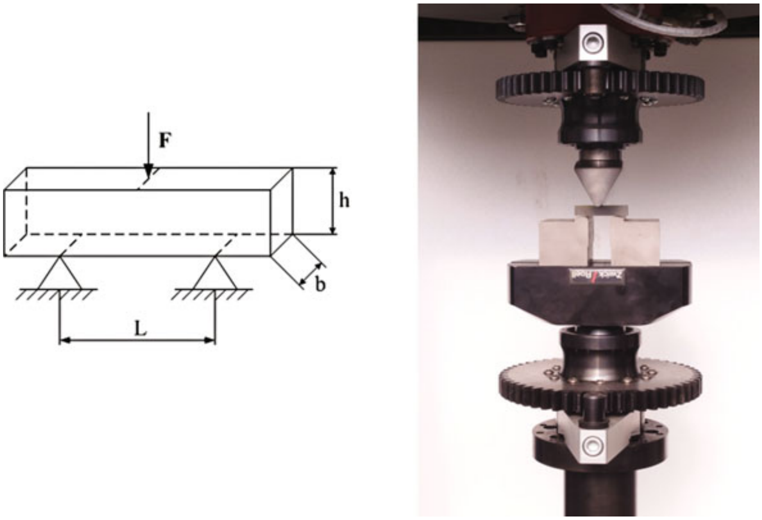

Fig. 2 A schematic drawing of the experimental sample dimensions for the three-point flexure σ_{omax} calculation and setting of the fatigue test

plotted from the measured values, which gives the relation between the maximum bending stress σ_{omax} and the number of cycles N_f.

Fractography analysis of broken samples was also carried out. For fractography analysis we used the scanning electron microscope TESCAN Vega II LMU. All fractography analyses were carried out in order to describe mechanisms of fatigue crack initiation, fatigue crack propagation and final static fracture of the samples.

3 Results and Discussion

For low-frequency fatigue testing we used 10 samples with simple blocky shape as seen in Fig. 2. Figure 3 shows the S-N curve of IN718 obtained from the three-point flexure fatigue tests at room temperature with a frequency of 150 Hz under the load ratio of $R = 0.11$. Obtained results were approximated using Eq. (2), which is Basquin's formula for the S-N presentation and approximation. This approach was also used for other materials [24].

$$\sigma_a = 2591 \times N_f^{-0.0811} \tag{2}$$

where $\sigma_f' = 2591$ is the coefficient of fatigue strength, and $-0.0811 = b$ is the lifetime curve exponent.

It is clearly seen from the measured S-N curve that the fatigue life increases with decreasing stress amplitude and the S-N curve appears to continuously decline as

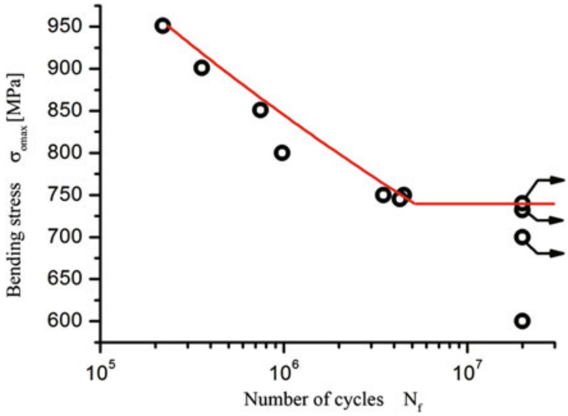

Fig. 3 The S-N curve for three-point flexure fatigue test of the Inconel alloy 718 with run-outs after reaching 2×10^7 cycles

the life extends. The limit number of cycles—2×10^7 (20,000,078)—was reached at the maximum banding stress σ_{omax} = 740 MPa. Accordingly, fatigue lifetime stress obtained using a different testing method—ultrasonic push-pull loading with $R = -1$ [25]—increases this factor by two fold higher (push-pull fatigue lifetime of about 386 MPa compared to three-point flexure fatigue lifetime of 740 MPa at the same number of cycles). Of course, these values may only roughly be compared because of different frequency of test and different mechanisms of loading.

From the three-point flexure fatigue tested samples we selected two samples as representatives for SEM observation to examine the fractured surface. Figure 4 shows an overall view of the fractured surfaces at different stress levels. Initiation sites are marked by an arrow. As a confirmation of the facts published in [26] at high stress levels as shown in Fig. 4a, fatigue cracks initiated from multiple initiation sites and resulted in a very small tensile final fracture area. With decreasing stress levels, the number of initiation sites decreases, as shown in Fig. 4b, controlled by the crystallographic slip at surface grains and, the static tensile final fracture area enlarges. This result is in good correlation with the results obtained at different fatigue loadings—ultrasonic push-pull and rotation bending loading. Fracture due to a single fatigue crack occurs in samples with longer fatigue life. Regardless of how high or low the stress levels are, all fatigue cracks initiate on free surfaces without a significant oxide or extrusion presence, even the presence of fish-eye commonly occurring in high frequency fatigue testing. After initiation, the fatigue crack propagates with transcrystalline mechanisms with typical striations, indicating the stable crack propagation as reported in Fig. 4c–d. The fatigue crack propagation mechanism is the same as in other fatigue loading (ultrasonic push-pull or rotation bending).

At higher stress levels, as shown in Fig. 4d–e, a major fatigue crack was generated and a few secondary cracks have appeared perpendicular to the main fatigue crack propagation, and probably situated at grain boundaries.

Figure 4f shows the change in the micro-mechanism of fractures from typical fatigue crack propagation and classical transcrystalline ductile dimpled fracture

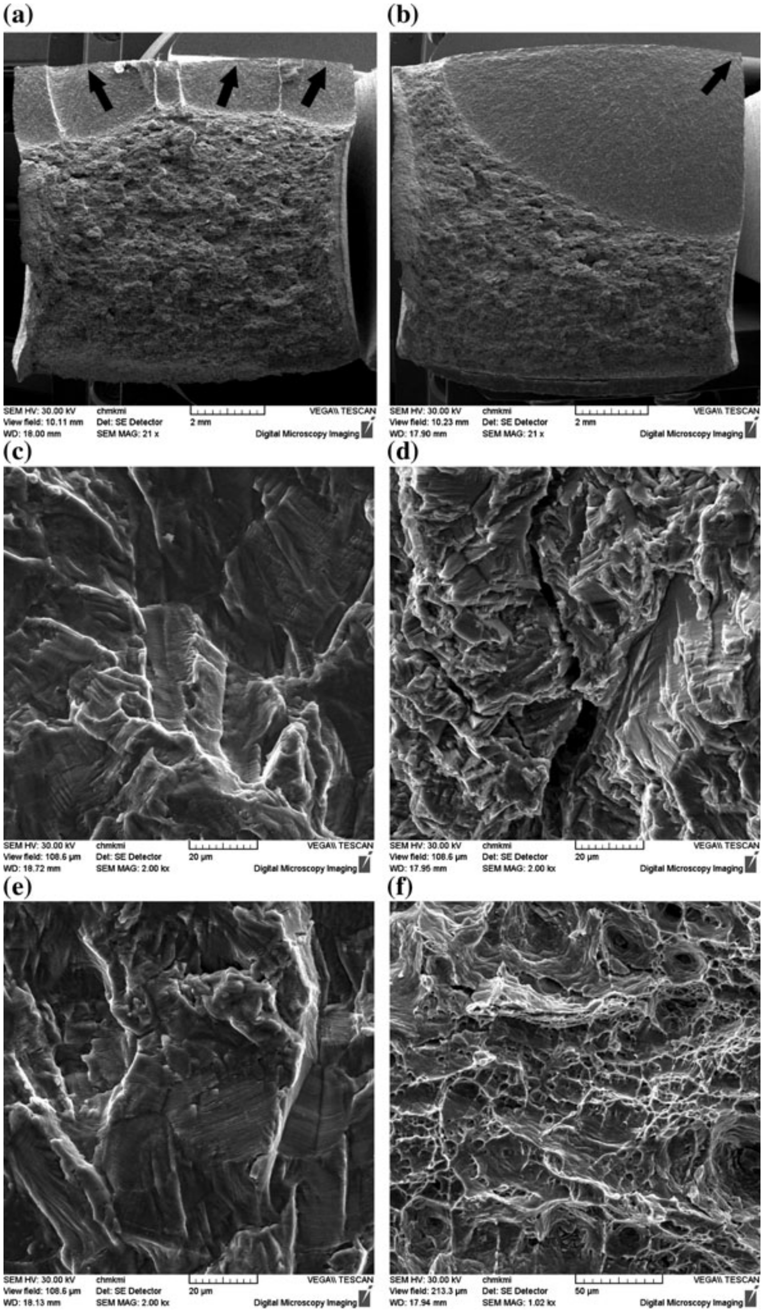
(a)
SEM HV: 30.00 kV
View field: 10.11 mm
WD: 18.00 mm
chmkmi
Det: SE Detector
SEM MAG: 21 x
2 mm
VEGA\\ TESCAN
Digital Microscopy Imaging
(b)
SEM HV: 30.00 kV
View field: 10.23 mm
WD: 17.90 mm
chmkmi
Det: SE Detector
SEM MAG: 21 x
2 mm
VEGA\\ TESCAN
Digital Microscopy Imaging
(c)
SEM HV: 30.00 kV
View field: 108.6 μm
WD: 18.72 mm
chmkmi
Det: SE Detector
SEM MAG: 2.00 kx
20 μm
VEGA\\ TESCAN
Digital Microscopy Imaging
(d)
SEM HV: 30.00 kV
View field: 108.6 μm
WD: 17.95 mm
chmkmi
Det: SE Detector
SEM MAG: 2.00 kx
20 μm
VEGA\\ TESCAN
Digital Microscopy Imaging
(e)
SEM HV: 30.00 kV
View field: 108.6 μm
WD: 18.13 mm
chmkmi
Det: SE Detector
SEM MAG: 2.00 kx
20 μm
VEGA\\ TESCAN
Digital Microscopy Imaging
(f)
SEM HV: 30.00 kV
View field: 213.3 μm
WD: 17.94 mm
chmkmi
Det: SE Detector
SEM MAG: 1.02 kx
50 μm
VEGA\\ TESCAN
Digital Microscopy Imaging

◀ **Fig. 4** SEM micrographs for fractography analysis of Inconel alloy 718 after three-point flexure fatigue test. An overall view of the fatigue crack initiation sites **a** $\sigma_{omax} = 900$ MPa, $N_f = 3.578 \times 10^5$; **b** $\sigma_{omax} = 750$ MPa, $N_f = 4.52 \times 10^6$. Fatigue crack propagation: **c** striation occurrence at $\sigma_{omax} = 800$ MPa, $N_f = 9.79 \times 10^5$, **d** major fatigue crack at $\sigma_{omax} = 850$ MPa, $N_f = 7.49 \times 10^5$ and **e** formation of secondary crack at $\sigma_{omax} = 850$ MPa, $N_f = 7.49 \times 10^5$, **f** the static fracture area with ductile dimple morphology

mechanism in the tensile final fatigue region. There is also a possibility to observe fractured NbC primary carbides. However, most of them are totally crushed, which confirms the fact about ductile mechanism of breaking in this region—pulling up the dimples till one massive crack occurs and causes the fracture.

4 Conclusions

The nickel-based superalloy INCONEL 718 is a well known material used for high temperature applications especially in the manufacturing of aero jet turbine discs. Many authors have carried out fatigue tests with rotation bending loading at room or elevated temperatures. Results of three-point bending fatigue tests are original and unique from this point of view. The three-point bending fatigue test was carried out at up to $\approx 2 \times 10^7$ cycles at room temperature. From fatigue testing, we obtained the following conclusions:

- Initiation of a fatigue crack is on a free surface without any oxide, carbide or other extrusion presence, or even fish-eye presence. At higher levels of stress, initiation occurs at multiple sites and with decreasing stress the initiation sites decrease to one single site. This is in good correlation with the results achieved by other authors who have carried out fatigue tests with different mechanisms of loading.
- Fatigue crack propagation is achieved via a transcrystalline mechanism with typical striation, and at higher stress levels the major crack forms together with small secondary cracks that are perpendicular to the crack propagation direction. The area of static tensile overload is characterised by ductile dimple morphology.

Fractography analysis shows a quite similar fatigue behaviour of this Inconel alloy 718 at three-point bending load and rotation bending load, even with high frequency ultrasonic push-pull loading. The only differences are in the form of initiation sites, which of course depends on the loading regime, and obtained different fatigue lifetime limits, where at three-point bending the fatigue lifetime is two times longer compared to ultrasonic push-pull loading at the same number of cycles.

Acknowledgments This work has been supported by Scientific Grant Agency of Ministry of Education of The Slovak Republic and the Slovak Academy of Sciences, No. 1/0533/15, No. 044ŽU-4/2014 and project EU ITMS 26110230117.

References

1. Paulonis DF, Oblak JM, Duvall DS (1969) Precipitation in nickel-base alloy 718. Trans ASM 62(3):611–622
2. Kirman I, Warrington DH (1970) The precipitation of Ni_3Nb phases in a Ni-Fe-Cr-Nb alloy. Metall Trans 1(10):2667–2675
3. Cozar R, Pineau A (1973) Morphology of y′ and y″ precipitates and thermal stability of Inconel 718 type alloys. Metall Trans 4(1):47–59
4. Oblak JM, Paulonis DF, Duvall DS (1974) Coherency strengthening in Ni base alloys hardened by DO_{22} γ' precipitates. Metall Trans 5(1):143–153
5. Sundararaman M, Mukhopadhyay P, Banerjee S (1992) Some aspects of the precipitation of metastable intermetallic phases in INCONEL 718. Metall Trans A 23(7):2015–2028
6. Slama C, Servant C, Cizeron G (1997) Aging of the Inconel 718 alloy between 500 and 750 ° C. J Mater Res 12(9):2298–2316
7. Radavich JF (1989) The physical metallurgy of cast and wrought alloy 718. In: Loria EA (ed) Superalloy 718—metallurgy and applications, The Minerals, Metals & Materials Society
8. Fournier D, Pineau A (1977) Low cycle fatigue behavior of Inconel 718 at 298 K and 823 K. Metall Mater Trans A 8(7):1095–1105
9. Reger M, Remy L (1988) High-temperature, low-cycle fatigue of IN100 superalloy influence of frequency and environment at high-temperatures. Mater Sci Eng A 101:55–63
10. Reger M, Remy L (1988) High-temperature, low-cycle fatigue of IN100 superalloy influence of temperature on the low-cycle fatigue behavior. Mater Sci Eng A 101:47–54
11. Bache MR, Evans WJ, Hardy MC (1999) The effects of environment and loading weaveform on fatigue crack growth in IN718. Int J Fatigue 21(1):69–77
12. Remy L, Alam A, Haddar N, Köster A, Marchal N (2007) Growth of small cracks and prediction of lifetime in high-temperature alloys. Mater Sci Eng A 468–470:40–50
13. Leo Prakash DG, Walsh MJ, Maclachlan D, Korsunsky AM (2009) Crack growth micro-mechanisms in the IN718 alloy under the combined influence of fatigue, creep and oxidation. Int J Fatigue 31(11–12):1966–1977
14. Pineau A (1989) Mechanisms of creep-fatigue interactions. In: Moura-Branco C, Guerra Rosa L (eds) Advances in fatigue science and technology. Kluwer Academic, Dordrecht
15. Alexandre F, Deyber S, Pineau A (2004) Modelling the optimum grain size on the low cycle fatigue life of a Ni based superalloy in the presence of two possible crack initiation sites. Scripta Mater 50(1):25–30
16. Masuda C, Tanaka Y (1986) Relationship between fatigue strength and hardness for high strength steels. Trans Jpn Soc Mech Eng Part A 52(476):847–852
17. Murakami Y, Kawakami K, Duckworth WE (1991) Quantitative evaluation of effects of shape and size of artificially introduced alumina particles on the fatigue strength of 1.5Ni–Cr–Mo (En24) steel. Int J Fatigue 13(6):489–499
18. Sakai T, Sakai T, Okada K, Furuichi M, Nishikawa I, Sugeta A (2006) Construction of electronic factual database on very high cycle fatigue properties for structural metallic materials. Int J Fatigue 28(11):1486–1492
19. Sakai T, Sato Y, Oguma N (2002) Characteristic S-N properties of high-carbon-chromium-bearing steel under axial loading in long-life fatigue. Fatigue Fract Eng Mater Struct 25(8–9):765–773
20. Wang QY, Bathias C, Kawagoishi N, Chen Q (2002) Effect of inclusion on subsurface crack initiation and gigacycle fatigue strength. Int J Fatigue 24(12):1269–1274
21. Wang QY, Kawagoishi N, Chen Q (2006) Fatigue and fracture behaviour of structural Al-alloys up to very long life regimes. Int J Fatigue 28(11):1572–1576
22. Yan N, Kawagoishi N, Chen Q, Wang QY, Nishitani H, Kondo E (2003) Fatigue properties of inconel 718 in long life region at elevated temperature. Key Engineering Materials. doi:10.4028/www.scientific. net/KEM.243-244.321

23. Chen Q, Kawagoishi N, Wang QY, Yan N, Ono T, Hashiguchi G (2005) Small crack behaviour and fracture of nickel-based alloy under ultrasonic fatigue. Int J Fatigue 27 (10–12):1227–1232
24. Trško L, Bokůvka O, Guagliano M, Nový F, Hazlinger M (2013) Ultra long fatigue life of 50CrMo4 steel with strengthened surface by high energy shot peening. In: Alfirević I, Semenski D (eds) 30th Danubia-Adria symposium on advances in experimental mechanics. Croatian Society of Mechanics, Zagreb
25. Belan J (2015) High frequency fatigue test of in 718 alloy—microstructure and fractography evaluation. Metalurgija—Metalurgy 54(1):59–62
26. Ma XF, Duan Z, Shi HJ, Murai R, Yanagisawa E (2010) Fatigue and fracture behavior of nickel-based superalloy Inconel 718 up to the very high cycle regime. J Zhejiang Univ Sci A (Applied Physics & Engineering) 11(10):727–737